WORLD JOURNAL OF PHARMACEUTICAL RESEARCH
SJIF Impact Factor 8.074
Volume 7, Issue 12, 491-505. Research Article ISSN 2277– 7105

ENHANCEMENT IN PHYSICAL PROPERTIES OF CD SUBSTITUTED COPPER FERRITE

[1]*C. M. Kale, [2]S. D. More, [1]M. K. Babrekar and [2]S. J. Shukla

[1]Department of Physics, Indraraj Arts, Commerce and Science College, Sillod-Aurangabad.

[2]Department of Physics, P.G. and Research Center, Deogiri College, Aurangabad (Maharashtra) India-431112.

Article Received on
21 April 2018,
Revised on 11 May 2018,
Accepted on 01 June 2018
DOI: 10.20959/wjpr201812-12526

***Corresponding Author**
C. M. Kale
Department of Physics, Indraraj Arts, Commerce and Science College, Sillod-Aurangabad.

ABSTRACT

The distinct compositions of $Co_{1-x}Cd_xFe_2O_4$ (x= 0.0, 0.1, 0.2, 0.3, 0.4, 0.5) samples were prepared by using sol-gel auto combustion method characterized to understand their physical and magnetic properties.The X-ray diffraction (XRD) analysis shows the existence of single phase cubic spinel structure with increase of lattice constant as Cd content increases. The bulk density, X-ray density, porosity, bond length and hopping length are exhibit similar behaviour. The particle size (< 33 nm) obtained from the Scherrer formula and linear intercept method using scanning electron microscope (SEM) confirms the nanocrystaline nature. Infrared (IR) shows two main absorption band corresponds to (A) and [B] site in spinel structure.

KEYWORDS: Sol-gel, X-ray diffraction, Lattice constant, Nanoferrite.

1. INTRODUCTION

Spinel ferrite is a class of commercially important materials because of their excellent electrical and magnetic property. The spinel ferrite materials having general formula $M-Fe_2O_4$ (M = Mn, Co, Ni, Zn, Mg, etc.), possess high electrical resistivity, low eddy current and dielectric losses. The spinel structure has been extensively dealt with by Gorter.[1] The unit cell of the ideal spinel structure is given in **Fig.1 (a)** and **(b)**.

The anions form a cubic closed pack in which cations partly occupy tetrahedral A-site and octahedral B-site interstices with space group O^7_h-F_3dm and present itself the cube formed by ferrite molecules and consisting of 32 of O^{2-} anions.[2]

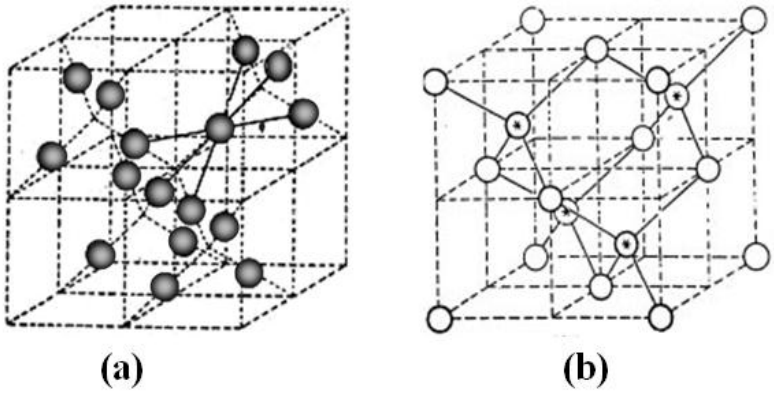

Fig.1: Unit cell of the ideal spinel structure.

Nanostructure spinel ferrite have attracted much attention in recent years due to their huge applications such as recording media, magnetic fluids, magnetic tape, microwave devices, transformers, gas sensor and actuators et al.[3-5] Pure cobalt ferrite and substituted cobalt ferrite has been widely studied due to its excellent physical and magnetic properties. Cobalt ferrite is a familiar hard magnetic material with high coercivity and good magnetostrictive properties among all the ferrite family. By the proper substitution and method of preparation it becomes soft material useful in many recent applications. The methods for preparation with proper composition plays very vital role in ferrite material formation. It is well known that several chemical methods are available for the preparation of ferrite; these include, Powder ceramic technique[6], Micro-emulsion method[7], Hydrothermal[8] Coprecipitation[9], citrate-gel method[10] and Sol-gel autocombustion[11] synthesis etc.

In the present study we used sol-gel autocombustion method. The advantages of this method are high purity; chemical homogeneity, small uniform particle size, saving energy, no reaction with containers, short processing time and low temperaturethus increase purity and minimize evaporation loss for the prepartaion of ultrafine uniform ferrite powder. Very fine ferrite powder can be produced by chemical co-precipitation and sol-gel method.[12-14]

Nanosized magnetic particles exhibit unique properties and have promissing technological applications in high density recording, colour imaging, ferrofluids, high frequency devices and magnetic refrigerators.[15] From the aplication point of view, the most significant properties of magnetic materials, namely magnetic saturation, coercivity, magnetisation and loss, change drastically as the size of the particle down into the nanometric range.[17-19] Among the different ferrite possess attractive properties for applications as soft magnet and low loss material at high frequencies.[20] Moreover there are numerous reports wherein

anomaly has been reported in the structural and magnetic properties of spinel ferite at nanoscale.[21,22]

To understand the relationship between structure, particle size and magnetic properties, it is essential to design a new magnetic material. In the present investigation we reports the divalent and nonmagnetic cadmium substituted cobalt ferrite, $Co_{1-x}Cd_xFe_2O_4$ (where, x= 0.0, 0.1, 0.2, 0.3, 0.4, 0.5) system was prepared by Sol-gel autocombustion technique. They were heated at low temperature 400^oC for 6 h to synthesize magnetic particle with varying particle size and study the nanosize effect on their physical properties. Cd substituted mixed ferrite is interesting from applications point of view and has not been studied much in detail. To the best of author's knowledge very few reports are avialable on study of divalent nonmagnetic Cd substituted Co-ferrite namely Abdeen et al, Ghani et al. 1991).[23,24]

The aim of the present work is to investigate the details of enhancement of physical properties of Cd^{2+} doped Co-ferrite nanoparticles. The substitution of Cd^{2+} ions for Fe^{3+} ions will improves the properties marked by similar to that of nonmagnetic substitution[25] used for any specific and characteristic applications.

2. EXPERIMENTAL

2.1. Material synthesis

The ultrafine samples of the magnetic nanoferrite with chemical formula $Co_{1-x}Cd_xFe_2O_4$ (where, x= 0.0, 0.1, 0.2, 0.3, 0.4, 0.5) were prepared by using sol-gel auto combustion method because of low processing temparature, good stoichimetric control, homogeneous distribution of reactant and production of ultrafine particles with narrow size distribution. The starting samples were taken in the form of high purity A. R. grade (>99%) for the praparation of ferrite nitrates as, cobalt nitrate-Co $(NO_3)0_2{\cdot}5H_2O$, cadmium nitrate-Cd $(NO_3)0_2{\cdot}4H_2O$, and ferric nitrate-Fe $(NO_3)0_2{\cdot}9H_2O$ all from s.d.fine-chem limited. The molar ratio of metal nitrates to citric acid was taken as 1:3. The metal nitrates were dissolved together in a minimum amount of double distilled water to get a clear solution. An aqueous solution of citric acid was mixed with metal nitrates solution, then ammonia solution was slowly added to adjust the pH at 7. The mixed solution was kept on to a hot plate and the solution is continuous stirred at 90^0C. During evaporation, the solution became viscous and finally formed a very viscous blackish-brown gel. When all water molecules were removed from the mixture, the viscous gel began frothing. After few minutes, the gel automatically ignited and

burnt with glowing flints. The decomposition reaction would not stop before the whole citrate complex was consumed. The auto-ignition was completed within a minute, yielding the black-colored ashes termed as a precursor. The obtained powder was then subjected to further heating treatment into a muffle furnace at relatively low temperature 400^{o}C for 6 h. The final product is then grinded and subjected to further study.

The steps of formation of ultrafine samples of the $Co_{1-x}Cd_xFe_2O_4$ nanoferrite as shown in the **Fig.2** photograph.

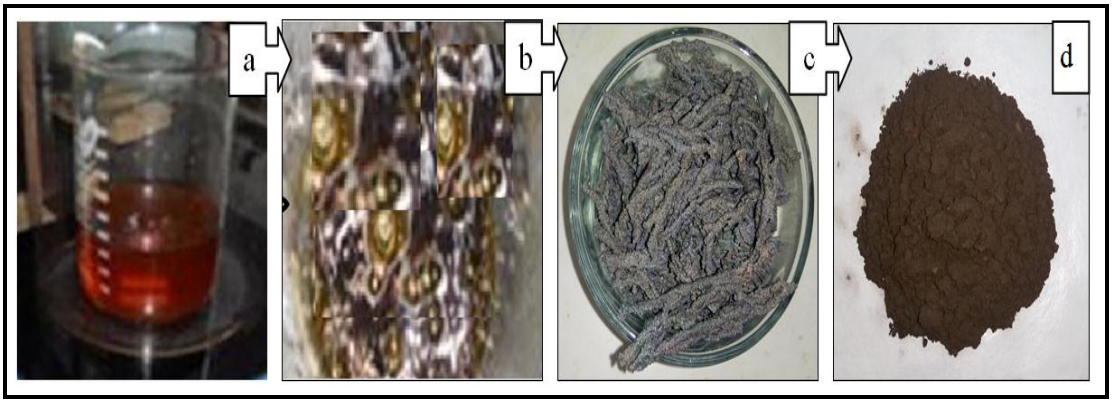

Fig.2: Pictorial steps of formation of ferrite nanoferrite $Co_{1-x}Cd_xFe_2O_4$ sample by sol-gel auto combustion method. (a) Sol solution at continuous heating and stirring, (b) Gel solution before ash, (c) Ash of ferrite material, (d) Fine sintered ferrite powder.

2.2. Characterization

The structural parameters were determined and confirmed by the X-ray diffraction (XRD) technique. XRD of all sample targeted with Cu-Kα (wavelength, λ= 1.5406 Å) was used to study the single phase nature and nano-phase formation of the Co-Cd ferrite system at room temperature by continuous scanning in the range of 20° to 80° by keeping rate 2 degree per minute. After confirmation of the structure of all the samples in the form of powders used to pellet form having dimensions 10 mm diameter and 2-3 mm thickness.

The particle size was calculted by using XRD pattern and Scherrer formula, also from Scanning Electron Micrograph (SEM) images. The micro structural analysis of the prepared samples was carried out by scanning electron microscopy. The infrared (IR) absorption spectra of all samples were recorded using IR spectrometer in the wave number range 700-300 cm^{-1} explain formation of two absorption band and site preference of the metal ions.

3. RESULTS AND DISCUSSION

3.1. Physical properties analysis

3.1.1. X-ray diffraction

X-ray diffraction (XRD) techniques is a basic techniques used to determine interplanar distances and lattice constant. Due to the random orientation of the crystallites in the sample, a reflection at the particular position is due to a set of atomic planes which are satisfying Bragg's diffraction law[26] given as,

$$2d\sin\theta = n\lambda$$

Where, d is the interpalner spacing, θ is the Bragg angle,n is the order of spectrum and λ is the wavelength of spectrum.

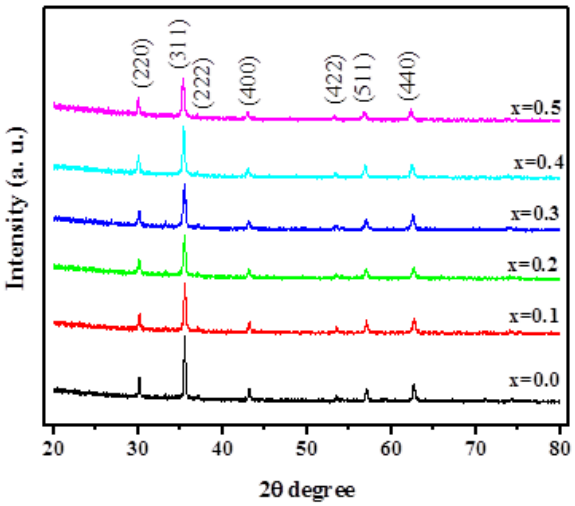

XRD patterns corresponding to $Co_{1-x}Cd_xFe_2O_4$ nanoferrite system for all x = 0.0, 0.1, 0.2, 0.3, 0.4 and 0.5 are recorded at room temperature and **Fig. 3** depicts the XRD pattern for all composition. All the peaks that appear in the diffraction patterns can be identified with the help of JCPDS data and from XRD, Bragg's peaks confirms the formation of single-phase cubic spinel structure as the corresponding planes such as (220), (311), (222), (400), (422), (511), and (440) are indexed by miller indices present in it. The strongest reflection comes from (311) plane that indicates spinel phase and the existence of broad peaks in the XRD patterns indicates the fine particle nature in nanosize dimensions of the prepared ferrite [27]. There are no any extra peaks observed means there is absence of any other impurity phase. All the peaks are reveals that the entire samples possess the single phase cubic spinel structure.

3.1.2. Lattice constant

Using XRD data, the lattice constant (a) is calculated by using the following relation,

$$a = d\sqrt{h^2 + k^2 + l^2} \quad Å$$

Where, all symbols carry their usual meanings.

The obtained values of the lattice constant (a) are lies in between 8.3652 Å to 8.3976 Å and listed in **Table 1.** It is clear that; the values of 'a' increases with increase in Cd^{2+} ions substitution as expected obeying Vegard's law.[28] This enhancement of lattice parameter is attributed to Cd^{2+} with larger ionic radius (1.03Å) which replaces Co^{2+} (0.82 Å) having smaller ionic radii. It is well-known that the distribution of cations on the octahedral B-sites and tetrahedral A-sites determines to a great extent the physical, electrical and magnetic properties of ferrites. There exists a correlation between the ionic radius and the lattice constant, the increase of the lattice constant is proportional to the increase of the ionic radius.[29,30]

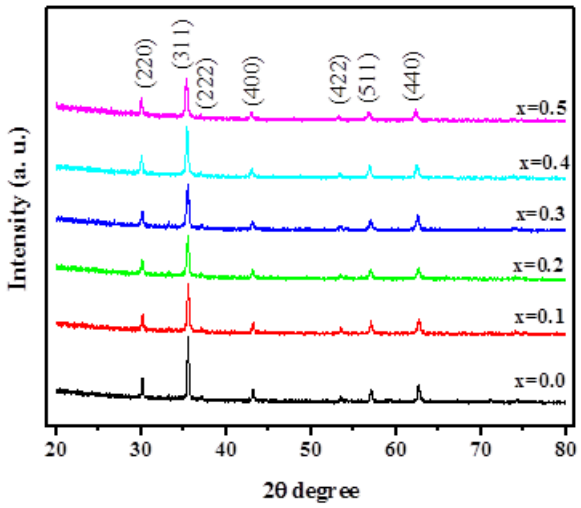

Cd content x	Lattice constant 'a' (Å)	Particle size 't' (nm)		Bulk density 'd' g/cm^3	X-ray density 'dx' g/cm^3	Percent porosity '% P'	absorption band frequency cm^{-1}	
		XRD	SEM				υ_1	υ_2
0.0	8.3652	33.27	33	3.523	5.324	33.83	546.54	448.33
0.1	8.3662	29.36	31	3.494	5.443	35.81	550.28	445.03
0.2	8.3738	29.35	29	3.441	5.549	38.00	552.00	440.00
0.3	8.3840	25.84	28	3.413	5.648	39.57	554.70	435.80
0.4	8.3951	27.72	26	3.404	5.747	40.77	558.50	421.04
0.5	8.3976	22.68	24	3.361	5.862	42.66	563.80	416.70

3.1.3. Particle size

The strucural morphology of XRD peaks is useful to find particle size. The average particle size (t in Å) of all sample compositions has been calculted from full width at half maximum (FWHM) the broadening of most intense paeks (311) using the classical Debye-Scherrer formula.[31]

$$t = \frac{k\lambda}{\beta \cos\theta} \quad Å$$

Where, λ is the X-ray wavelength (=1.5405Å) of radiation, k is the shape factor with typical value 0.94, β is the line broadening at FWHM of the diffraction peak and θ is the diffraction angle in radian.

The values of particle size obtained from XRD data and SEM are given in **Table 1**. The average particle sizes is found in the range ~22 to 33nm which are close to the results obtained from SEM images and good agreement with report of Sonal Singhal et.al.[32]

3.1.3. The bulk density

The bulk or apperent density (d) of all the samples was calculated by putting the values mass and volume of the pellet in the following relation.

$$d = \frac{m}{\pi r^2 h} \quad g/cm^3$$

Where, m, r and h are mass, radius and thickness of the pellet respectively.

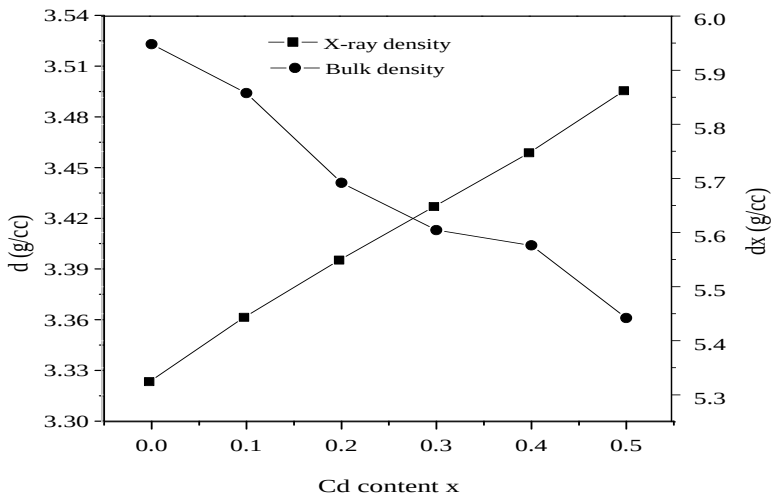

Fig.4: Variation of X-ray density (dx) and Bulk density (d) with Cd content x in $Co_{1-x}Cd_xFe_2O_4$ ferrite system.

It is observed from **Table 1** and **Fig. 4** that the values of bulk density of each sample are less than X-ray density. As Cd content increases then bulk density decrease and X-ray density increase, due to high density of Cd metal.[33] This may be also due to the existence of pores, which were formed and developed during the sample preparation or sintering process. The X-ray density and bulk density increase significantly with increase in Cd content.

3.1.3. The X-ray density

The X-ray density (dx) of all the samples was calculated using the molecular weight and volume of the unit cell using the following relation.

$$dx = \frac{ZM}{Na^3} \quad g/cm^3$$

Where, Z is the number of atom per unit cell (=8), M is molecular weight, N is Avogadro's number and 'a' is lattice constant.

The values of X-ray density obtained from above equation and listed in **Table 1**. The curve of X-ray density with Cd content x is as shown in **Fig.4.** It is observed that the X-ray density increases with substitution of Cd^{2+} ions. The increase in X-ray density is attributed to the facts that increase in mass over take the decrease in volume of the unit cell and the atomic weight of Cd (112.40) is higher than of Co (58.93). The increase in X-ray density is directly proportional to with the substitution of Cd^{2+} ions in cobalt ferrite.

3.1.4. Percent porosity

The percentage porosity (% P) of the samples is calculated using the following relation and listed in **Table 1**.

$$\%P = \left(1 - \frac{d}{dx}\right) \times 100$$

Where, d is the bulk density, dx is the X-ray density. The calculated values of % P are increases from 33.83 to 42.66% with increase in Cd content x. Moreover, the change in the porosity for all investigated samples is due to the change in the X-ray density; another reason might be the difference in the melting point of the nitrate used.[34] The increasing values of porosity suggest that the prepared sample becomes porous with increase in Cd content increases. such types of material are generally used for sensors and coating technology.[35]

3.1.5. Bond length

Bond lengths R_A and R_B are the shortest distance between A-site and B-site cations with the oxygen ion respectively.

Table. 2: Values of bond length, hopping length, tetrahedral and octahedral bond length and, shared tetrahedral and octahedral edge of $Co_{1+x}Cd_xFe_2O_4$ ferrite (x=0.0 to 0.5) system.

Cd Content x	Bond length (Å)		Hopping length (Å)		d_{Ax} (Å)	d_{Bx} (Å)	d_{AxE} (Å)	d_{BxE} (Å)	d_{BxEU} (Å)
	R_A	R_B	L_A	L_B					
0.0	1.8980	2.0405	3.6221	2.9579	3.1000	2.8152	2.9592	1.9560	2.0076
0.1	1.8982	2.0407	3.6226	2.9583	3.1003	2.8155	2.9596	1.9562	2.0079
0.2	1.8999	2.0426	3.6259	2.961	3.1032	2.8181	2.9623	1.9580	2.0097
0.3	1.9023	2.0451	3.6303	2.9646	3.1070	2.8215	2.9659	1.9603	2.0122
0.4	1.9048	2.0478	3.6351	2.9685	3.1111	2.8252	2.9699	1.9629	2.0148
0.5	1.9053	2.0484	3.6362	2.9694	3.1120	2.8261	2.9707	1.9635	2.0154

The variation of the bond length R_A and R_B calculated by using the relations equation given below[36] and listed in **Table 2.**

$$R_A = a\sqrt{3}\left(\delta + \frac{1}{8}\right) \text{ and}$$

$$R_B = a\left(3\delta^2 - \frac{\delta}{2} + \frac{1}{16}\right)^{1/2}$$

Where, δ= (u-0.375) and u is the oxygen positional parameter.

The values R_B are greater than R_A indicates that the B-site cations Co^{2+} are closer to oxygen O^{2-} ions exerts more attractive force. Also Cd^{2+} is nonmagnetic in behavior so atoumatically it pushed to Fe^{3+} ions present at A-site.[37]

3.1.6. Hopping length

The hopping length between magnetic ions in the tetrahedral A-site 'L_A' and octahedral B–site'L_B' be calculated by the foloowing equations are,[38,39]

$$L_A = 0.25\, a\sqrt{3} \quad Å$$

$$L_B = 0.25a\sqrt{2} \quad Å$$

The estimated values of L_A and L_B as a function of Cd content x are given in **Table 2** shows that the distance between the magnetic ions L_A increases from 3.6221 to 3.6362 Å and L_B increases from 2.9579 to 2.9694 Å as the Cd^{2+} ions content increases. This may be explained

on the basis of difference in ionic radii of constituent ions Cd^{2+} (1.03 Å) and Co^{2+}(0.82 Å). The behavior of ion jump lengths is attributed to variation of lattice constant with Cd content x.

3.1.7. Tetrahedral and octahedral bond length

The bond length of tetrahedral (A) site 'd_{Ax}' (shortest distance between A-site cation and oxygen ion) and octahedral [B] site 'd_{Bx}'(shortest distance between B-site cation and oxygen ion), tetrahedral edge d_{AXE}, shared octahedral edge 'd_{BXE}' and unshared octahedral edge 'd_{BXEU}' calculated by using the values of lattice constant 'a' and oxygen positional parameter 'u', in the following equations.

$d_{Ax} = a \sqrt{3} (u-1/4)$

$d_{Bx} = a [3u^2-(11/4)u+43/64)]^{1/2}$

$d_{AxE} = a \sqrt{2} (2u-1/2)$

$d_{BxE} = a \sqrt{2}(1-2u)$

$d_{BxEU} = a [4u^2 – 3u + (11/16)]^{1/2}$

The values calculated from above mentioned expression are presented in **Table 2** and represented in **Fig.5**. The **Table 2** indicates that the tetrahedral bond length d_{AX} and octahedral bond length d_{BX} increases as Cd^{2+} content 'x' increases. Also shows that the tetrahedral edge 'd_{AXE}', 'd_{BXE}' unshared octahedral edge 'd_{BXEU}' does not vary much with composition while shared octahedral edge 'd_{BXE}'increases.[40]

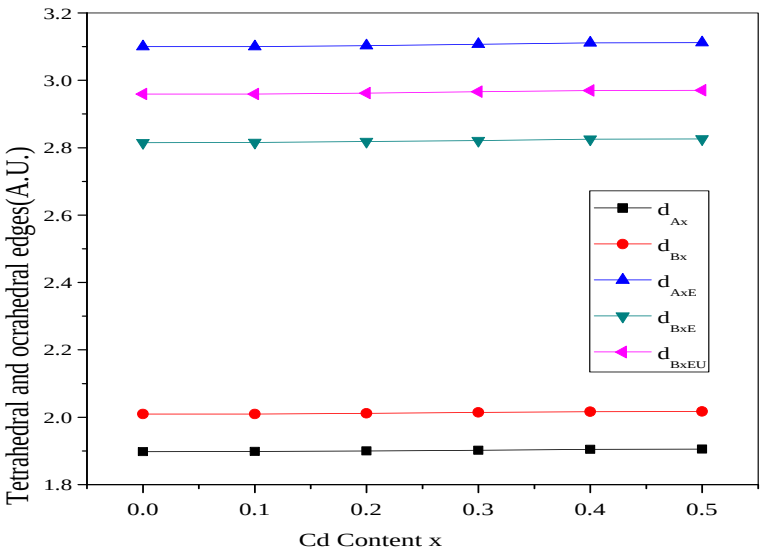

Fig. 5: Variation of tetrahedral and octahedral bond length, shared tetrahedral and octahedral edge of $Co_{1-x}Cd_xFe_2O_4$ ferrite system.

3.2. Infra Red analysis

Infra Red (IR) spectroscopic analysis is an additional tool for the structural characterization. IR technique is extremely competent in the form of infrared spectrum used as a fingerprints obtained in a transmittance (%) of the IR radiation plotted against wavenumber. The infrared spectra for all prepared samples of $Co_{1-x}Cd_xFe_2O_4$ nano ferrite system are shown in **Fig.6**.

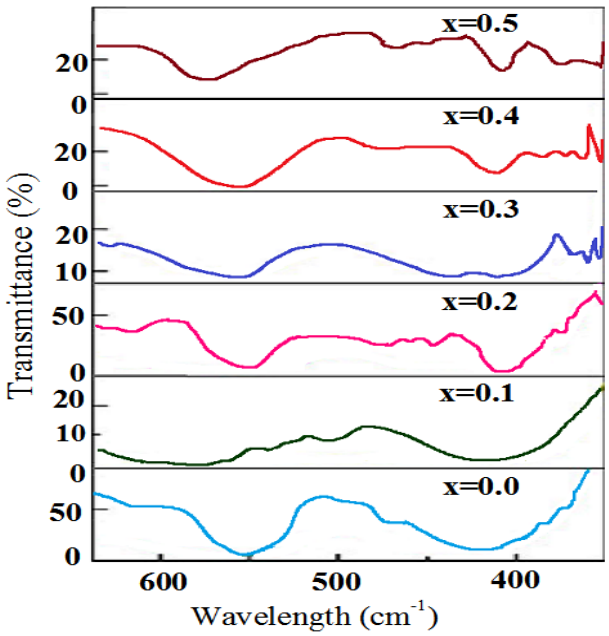

Fig. 6: IR spectra of $Co_{1-x}Cd_xFe_2O_4$ nanoferrite system.

According to Waldron[41] the ferrites can be considered continuously bonded crystals, meaning that the atoms are bonded to all nearest neighbour by equivalent forces. In ferrites the metal ions are situated in two different sublattices designated tetrahedral (A-site) and octahedral (B-site) according to the geometrical configuration of the oxygen nearest neighbours. Waldron[41] and Hafner[42] have attributed the band around 600 cm^{-1} and 400 cm^{-1}. In the present study the absorption spectra shows two major absorption bands i.e. higher absorption band (υ_1) lies in the range of 546.54 to 563.80 cm^{-1} and lower absorption band (υ_2) in the range 448.33 to 416.70 cm^{-1} are assigned to the tetrahedral [B] and octahedral (A) sites. The values of absorption bands (υ_1 and υ_2) are presented in **Table 1** shows that υ_1 goes on increasing while υ_2 decreases with increase in Cd^{2+} content. The difference in frequencies of υ_1 and υ_2 is due to changes in the bond length Fe^{3+}-O^{2-} at tetrahedral and octahedral sites.[43] The remaining bands are probably due to combinational frequencies or overtones. The nature of absorption bands in the infrared spectra depends on the distribution and type of cations among octahedral and tetrahedral sites.[44]

3.3. Scanning Electron Morphology (SEM)

The scanning electron microscopy (SEM) is one of the powerful techniques used to analyze the microstructure of ferrites. External morphology of heterogeneous materials on nanoscale can be observed and characterized by SEM, obtaining magnified three-dimensional-like images of their surfaces.

The SEM micrograph of fractural surface of typical sample of Cd-sustituted $Co_{1-x}Cd_xFe_2O_4$ (where, x= 0.1, 0.2) ferrite system are presented in **Fig.0.7.** The particle size was also determined from SEM images by linear intercept method using the formula.[45]

$$Ga = \frac{1.5L}{MN}$$

Where, L is total test line length, M is magnification and N is the total number of intercepts.

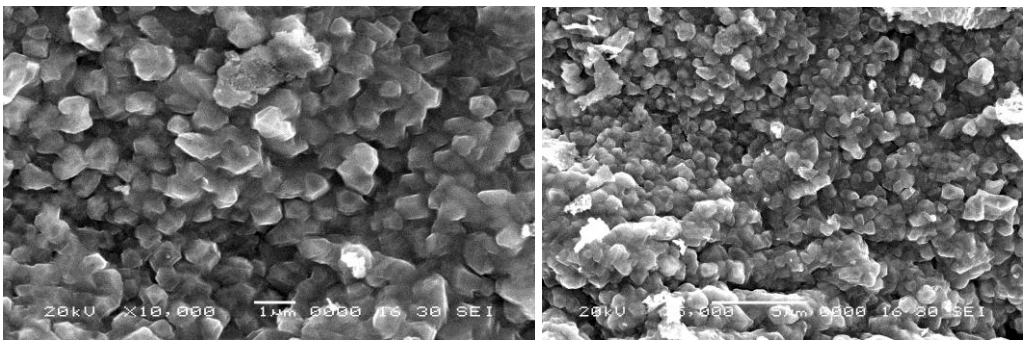

x=0.1 **x=0.2**

Fig. 7: SEM of typical sample $Co_{1-x}Cd_xFe_2O_4$ (where, x= 0.1, 0.2) ferrite system.

The morphology of particle is almost uniform shape in cubical grains is progressively increased with increasing Cd^{2+} ions. The particle size obtained from SEM are varies in between 24 to 33 nm and the obtained values are given in **Table 1**. It is evident from SEM images microstructure affected by Cd^{2+} ions concentration as well as by method of preparation. It can be observed that the prepared samples are porous in nature. Small amount of pores in SEM images revels that the sintering is done in a satisfactory manner. The effect of increasing Cd-content on investigated samples is the enhancement of the grain growth as seen from the scanning electron micrographs.

4. CONCLUSIONS

To enhance the physical and magnetic properties of The Nano-crystalline cadmium substituted cobalt ferrite $Co_{1-x}Cd_xFe_2O_4$ (where, x= 0.0, 0.1, 0.2, 0.3, 0.4, 0.5) system were successfully synthesized by using sol-gel auto combustion technique. The XRD pattern

shows the formation of cubic spinel structure of all the samples. The particle size calculated by the Sherrer formula is in 24 - 33 nm range. The lattice constant increases with increses in cadmium content. Values of L_A and L_B varies with respect to lattice constant. The values of tetrahedral and octahedral bond length, shared tetrahedral and octahedral edge are good agreement with the previous report. IR analysis is shows two absorption band ~ 600 cm^{-1} and 400 cm^{-1} depends on the distribution and type of cations among octahedral and tetrahedral sites. SEM study reveals that the paricle size of all the samples is in nanometer dimension.

5. ACKNOLWEDGEMENT

The author (CMK) is thankful to Dr. Babasaheb Ambedkar Marathwada University, Aurangabad for providing minor research project grant. And also deep thanks to Professor K. M. Jadhav, Department of Physics, Dr. Babasaheb Ambedkar Marathwada University, Aurangabad (M.S.) India; for his fruitful discussion and providing laboretory facilities.

REFERENCES

1. E.W. Gorter, C. O. Arean, J. Chem. Soc. Dalton Trans, 1985; 2155.
2. T. R. Mehdiyev, N. R. Babayeva, A. M. Gashimov, A. A. Habibzade. Fizika, 2008; 2(14): 80-88.
3. Dong S. X., Li JF, Viehland D. Appl Phys Lett., 2004; 84: 4188–4191.
4. Semenov A. A, Karmanenkov S.F., Demidov V.E., Kalinikos B.A., Srinivasan G., Slavin A.N., Mantese J.V. Appl Phys Lett., 2006; 88: 033503.
5. N. Rezlescu, E. Rezlescu, F. Tudorache, P. D. Popa, Romanian Reports in Physics, 2009; 61(2): 223–234.
6. C. M. Kale, P. P. Bardapurkar, S. J. Shukla, K. M. Jadhav, J. Magn. Magn. Mater., 2013; 331: 220–224.
7. M. J. Iqbal and M. R. Siddiquah, J. Alloys Compounds, 2007; 453: 513-518.
8. J. Wan, Y. Yao, and G. Tang, Appl. Phys. A., 2007; 89: 529.
9. Hassan, A., Khan, M. A., Shahid, M., Asghar, M., Shakir, I., Naseem, S. and Warsi, M.F. J. Magn. Magn. Mater, 2015; 393: 56-61.
10. P. P. Hankare, U. B. Sankpal, R. P. Patel, P. D. Lokhande and R. Sasikala, Mater. Sci. Engg: B., 2011; 176(2): 103-109.
11. Vinod N. Dhage, M. L. Mane, M. K. Babrekar, C. M. Kale, K. M. Jadhav, J. Alloys. Compounds, 2011; 509: 4394-4398.
12. P. C. Kau, T. S. Tsai, J. Appl. Phys, 1989; 65: 4349.

13. C. J. Chen, K. Bridger, S. R. Winzer, V. Paivernekar, J. Appl. Phys., 1998; 63: 3786
14. C. H. Lin, S.Q. Chen. J. Mater. Sci., 1983; 15: 31
15. W. C. Kim, S.L. Park, S. J. Kim, S. W. Lee, C. S. Kim. J. Appl. Phys, 2000; 87: 6241.
16. M. Kishimoto, Y. Sakurai, T. Ajima, J. Appl. Phys., 1994; 76: 7506.
17. J.L. Dorman, D. Fiorani (Eds.), Magnetic Properties of Fine Particles, North-Holland, Amsterdam, 1992.
18. M. L. Bilas, A. Chatelain, W.A. de Heer, Science, 1994; 265: 1682. D.D.
19. Aswehalom, D.P.D. Vincevzo, Physics Toady, 1995; 43.
20. J.Shi, S. Glder, K.Babcock, D.D. Aswehalom, Science, 1996; 271: 937.
21. S.Son, M. Taheri, E.Carpenter, V.G.Harris, M.E. Mc Henry, J. Appl. Phys, 2002; 91(10): 7589.
22. H. Ehrhardt, S. J. Campbell, M.Hofmann, J. Alloys. Compounds, 2002; 339: 255.
23. V.Sepelak, K. Tkacova, V.V. Boldyrev, S. Wibmann, K.D. Becker, Physica B., 1997; 617: 234.
24. Abdeen, A. M., O. M. Hemeda, E. E. Assem and M. M. El-Sehly. J. Magn. Magn. Mater, 2002; 238: 75.
25. A.Ghani, A. A. Sattar and J. Pierre. J. Magn. Magn. Mater., 1991; 97: 141.
26. H. Anwar, Asghari Maqsood J. Magn. Magn. Mater., 2013; 333: 46–52.
27. Charles Kittel, Introduction to Solid State Physics, VII Edn, John Wiley and Sons, 2009; 29.
28. Hankare P. P., Patil R. P., Sankpal U. B., Jadhav S. D., Mulla I. S., Jadhav K. M., Chougule B. K. J. Magn. Mag. Mater, 2009; 321(19).
29. Vegard, L. Die Konstitution Der Mischkristalle Und die Raumfüllung Der Atome. Zeitschrift für Physik, 1921; 5: 17.
30. Globus, A., H. Pascard and V. Cagan. J. Physique (call), 1977; 38: C1-163)
31. S. R. Bainade, C. M. Kale, M. C. Sable, J. Supercond. Nov. Magn, July 2017.
32. Cullity B. D., Stock S. R., Elements of X-ray diffraction (New York, Prentice Hall), 2001; 154.
33. Sonal Singhal, Sheenu Jauhar, Kailas Chandra, Sandeep Bansal. Bull. Mater. Sci., 36(1): 107-114.
34. Saroaut Noor, S.S. Sikder, M. Samir Ullah1, M.A. Hakim, Shireen Akhter Journal of Bangladesh Academy of Sciences, 2011; 35(2): 229-235.
35. M.A. Ahmed, N.Okasha and S. I. El-Dek, Nanotechnology, 2008; 19: 065603 (6).
36. N. Bagum, M.A. Gafur, A.H. Bhuiyan D.K. Saha, Phys. Status Solidi A, 207: 986.

37. Standley K. J., 1972, Oxide Magnetic Material, Oxford, U. K. Clarendon.
38. S. P. Dalawai, T. J. Shinde, A. B. Gadkari, P. N. Vasambekar Bull. Mater. Sci., October 2013; 36(5): 919–922.
39. R. H. Kadam, S. S. More, A. B. Kadam, D. R. Mane, G. K. Bichile Open Chem., 2010; 8: 419.
40. A.T. Raghavender, K. M. Jadhav Int. J. Mod Phys B., 2009; 23: 223.
41. R. K. Sharma, V. Sebastian, N. Lakshmi, K. Venugopalan, V. R. Reddy, A. Gupta, Phy. Rev. B., 2007; 75: 144419.
42. R.D. Waldron, phys. Rev., 1955; 99.
43. S.T. Hafner, Z. Krist., 1961; 115: 331.
44. V.A. Potakova, W. D. Zverv and V. P. Romanov, Physics Status Solidi (A), 1972; 12: 623.
45. M. Raghasudha, D. Ravinder, P. Veerasomaiah, Nanoscience and Nanotechnology, 2013; 3(5): 105-114.
46. Wurst J.C., Nelson J. A. Am. Ceram. Soc. Bull, 1972; 55: 109.